11th World Congress on Computational Mechanics (WCCM XI)
5th European Conference on Computational Mechanics (ECCM V)
6th European Conference on Computational Fluid Dynamics (ECFD VI)
E. Oñate, J. Oliver and A. Huerta (Eds)

ON THE COSSERAT-CAUCHY HOMOGENIZATION PROCEDURE FOR HETEROGENEOUS PERIODIC MEDIA

D. Addessi*[1], M.L. De Bellis[1], E. Sacco[2]

[1] Dip. di Ingegneria Strutturale e Geotecnica,
Universitá di Roma "Sapienza", Via Eudossiana 18, 00184, Roma, Italy
[2] Dip. di Ingegneria Civile e Meccanica,
Universitá di Cassino e del Lazio Meridionale, Via G. Di Biasio 43, 03043, Cassino (FR), Italy
daniela.addessi@uniroma1.it, marialaura.debellis@uniroma1.it,
sacco@unicas.it

Key words: Heterogeneous periodic materials, Cosserat continuum, Kinematic map, Perturbation displacements, Constitutive identification.

Abstract. In the present paper the homogenization problem of periodic composites is investigated, in the case of a Cosserat continuum at the macro-level and a Cauchy continuum at the micro-level. In the framework of a strain-driven approach, the two levels are linked by a kinematic map based on a third order polynomial expansion. The determination of the displacement perturbation fields in the Unit Cell (UC), arising when second or third order polynomial boundary conditions are imposed, is investigated. A new micromechanical approach, based on the decomposition of the perturbation fields in terms of functions which depend on the macroscopic strain components, is proposed. The identification of the linear elastic 2D Cosserat constitutive parameters is performed, by using a Hill-Mandel-type macrohomogeneity condition. The influence of the selection of the UC is analyzed and some critical issues are outlined. Numerical examples referred to a specific composite with cubic symmetry are shown.

1 INTRODUCTION

This work is framed in the context of computational homogenization techniques for periodic composites adopting different continua at the two scales of interest: a Cosserat continuum at the macro-level and a Cauchy continuum at the micro-level [1, 2]. On one side, the adoption of a generalized continuum model at the macro-level allows to overcome the intrinsic limit of the Cauchy theory that is insensitive to length scale parameters [3, 4, 5, 6], on the other side the adoption of the classical Cauchy continuum at the microscopic level is motivated by the fact that nonlinear constitutive relationships are well-established in this framework. The presented computational homogenization procedure is based on an idea proposed in [3], in which a polynomial kinematic map was

derived to link the two levels. In particular, the displacement field at the micro-level is represented as the superposition of the kinematic map and an unknown perturbation field, arising as a consequence of the heterogeneous nature of the material. To be noted is that the procedure discussed in [3] has some drawbacks, as remarked in [7], lacking in satisfying the balance equations in the case of a homogenized material.Furthermore, when the Cosserat macroscopic strain components are applied to the UC, the perturbation fields are no longer periodic, as instead in the case of Cauchy macroscopic strains. In [2] a revision of the above procedure is presented, proposing some improvements for overcoming the highlighted limits, but still leaving open questions. To this end, aimed at a more accurate determination of the perturbation displacement fields, a new procedure is herein established. A three steps homogenization procedure is proposed, on the basis of the micromechanical approach presented in [8], where a technique grounded on asymptotic approach is used and a second gradient continuum is employed at the macroscopic level. Herein, the original idea presented in [8] is extended to the case of a 2D Cosserat continuum at the macro-level, expressing the perturbation field in function of the first, second and third gradients of the kinematic map. In order to verify the effectiveness of the proposed procedure for Cosserat continuum, the distribution of the perturbation fields on a single UC is compared with the results carried out for a RVE, which is derived by arranging a large number of UCs.

In the case of the homogenization procedure herein adopted, a further debated issue is the identification of the effective constitutive parameters. In fact, due to the lack of a direct correspondence between strain and stress components at the two levels (Cosserat and Cauchy), some problems arise. Different approaches were proposed, each with distinct advantages and limits. Several authors derive the homogenized constitutive components starting from the generalized Hill-Mandel macrohomogeneity condition, whether they consider a Cosserat [3, 1] or a second-order [4] continuum at the macro-level. The evaluation of the macroscopic stresses is obtained as the weighted average of microscopic stresses over the volume. The microscopic coordinates work as weighting functions, leading in some cases to not physically consistent results [8]. For example, higher order constitutive components are identified also when a homogeneous elastic material at the micro-level is considered.

Although the well-known limits, the generalized Hill-Mandel macrohomogeneity condition is used in this work, to identify the linear elastic homogenized coefficients of the Cosserat continuum adopted at the macro-level. A simple periodic composite medium is considered, by focusing on the influence of the selection of the UC. A critical interpretation of the obtained results is provided.

2 Cosserat-Cauchy homogenization

The computational homogenization procedure, herein discussed, adopts the Cosserat continuum at the macro-level and the Cauchy medium at the micro-level. According to the classical Cosserat formulation for 2D media, at the typical macroscopic material point

$\mathbf{X} = \{X_1,\, X_2\}^T$, the displacement vector $\mathbf{U} = \{U_1,\, U_2,\, \Phi\}^T$ is defined, where U_1 and U_2 are the translational degrees of freedom and Φ is the rotational one. The Cosserat strain vector is partitioned into three sub-vectors as follows:

$$\mathbf{E} = \left\{ \begin{array}{c} \bar{\mathbf{E}} \\ \mathbf{K} \\ \Theta \end{array} \right\}, \tag{1}$$

where $\bar{\mathbf{E}}$ collects the axial and symmetric shear strains, $\mathbf{K}$ is the vector collecting the curvature components, and Θ is the skew-symmetric shear component, defined as :

$$\bar{\mathbf{E}} = \left\{ \begin{array}{c} E_1 \\ E_2 \\ \Gamma_{12} \end{array} \right\} = \mathbf{L} \left\{ \begin{array}{c} U_1 \\ U_2 \end{array} \right\}; \quad \mathbf{K} = \left\{ \begin{array}{c} K_1 \\ K_2 \end{array} \right\} = \nabla\Phi; \quad \Theta = \Phi - \mathbf{S}^T \left\{ \begin{array}{c} U_1 \\ U_2 \end{array} \right\}. \tag{2}$$

where $\mathbf{L}$, ∇ and $\mathbf{S}$ are:

$$\mathbf{L} = \left[\begin{array}{cc} \dfrac{\partial}{\partial X_1} & 0 \\ 0 & \dfrac{\partial}{\partial X_2} \\ \dfrac{\partial}{\partial X_2} & \dfrac{\partial}{\partial X_1} \end{array} \right]; \quad \nabla = \left\{ \begin{array}{c} \dfrac{\partial}{\partial X_1} \\ \dfrac{\partial}{\partial X_2} \end{array} \right\}; \quad \mathbf{S} = \left\{ \begin{array}{c} -\dfrac{\partial}{\partial X_2} \\ \dfrac{\partial}{\partial X_1} \end{array} \right\}. \tag{3}$$

Consistently with the strain driven approach, the macroscopic strain components, evaluated at $\mathbf{X}$, are used as input variable for the microscopic level. Indeed, the BVP at the micro-level is stated by defining a kinematic map expressed in function of the vector $\mathbf{E}$.

Considering a periodic medium, a repetitive UC, containing all the necessary information regarding the material and geometrical properties of the composite, can be selected for the micromechanical and homogenization analyses. In particular, a rectangular UC is analyzed, whose size is $a_1 \times a_2$ and its center is located at the macroscopic point $\mathbf{X}$, being characterized by the displacement field $\mathbf{u} = \{u_1,\, u_2\}^T$, defined at each point $\mathbf{x} = \{x_1,\, x_2\}^T$ of the UC domain ω.

The following representation form, typical of the first order homogenization scheme, where the Cauchy model is used at both the macro- and micro-level, is assumed for the displacement field solution of the BVP at the typical point $\mathbf{x}$ of the UC:

$$\mathbf{u}\left(\mathbf{X}, \mathbf{x}\right) = \mathbf{u}^*\left(\mathbf{X}, \mathbf{x}\right) + \widetilde{\mathbf{u}}\left(\mathbf{X}, \mathbf{x}\right) \tag{4}$$

in which the dependence on the macroscopic and microscopic coordinates, $\mathbf{X}$ and $\mathbf{x}$, is indicated. According to Eq. (4), the displacement is expressed as the superposition of an assigned field $\mathbf{u}^*\left(\mathbf{X}, \mathbf{x}\right)$, i.e. the kinematic map, depending on the macro-level deformation vector $\mathbf{E}$, and a perturbation field $\widetilde{\mathbf{u}}\left(\mathbf{X}, \mathbf{x}\right)$. The strain vector at the microscopic level is

derived by applying the kinematic operator defined for the 2D Cauchy problem and, in expanded form, it results as:

$$\boldsymbol{\varepsilon} = \left\{ \begin{array}{c} \varepsilon_1 \\ \varepsilon_2 \\ \gamma_{12} \end{array} \right\} = \mathbf{l} \left\{ \begin{array}{c} u_1 \\ u_2 \end{array} \right\} \qquad \text{with } \mathbf{l}\left(\mathbf{x}\right) = \left[\begin{array}{cc} \bullet_{,1} & 0 \\ 0 & \bullet_{,2} \\ \bullet_{,2} & \bullet_{,1} \end{array} \right] , \tag{5}$$

where $\bullet_{,i}$ indicates the partial derivative with respect to x_i. A key point of the procedure is the definition of a suitable kinematic map, i.e. the form of the assigned field $\mathbf{u}^*\left(\mathbf{X},\mathbf{x}\right)$ in function of the macroscopic strain variables. The different nature of the continua coupled at the two levels makes this step not straightforward. In what follows, the map proposed in [2], formulated for a 2D orthotropic homogenized medium, is adopted. In particular, in compact form it can be written as:

$$\mathbf{u}^*\left(\mathbf{X},\mathbf{x}\right) = \mathbf{A}^1\left(\mathbf{x}\right)\overline{\mathbf{E}}\left(\mathbf{X}\right) + \mathbf{A}^2\left(\mathbf{x}\right)\mathbf{K}\left(\mathbf{X}\right) + \mathbf{A}^3\left(\mathbf{x}\right)\Theta\left(\mathbf{X}\right) = \mathbf{A}\left(\mathbf{x}\right)\mathbf{E}\left(\mathbf{X}\right) , \tag{6}$$

where

$$\mathbf{A}\left(\mathbf{x}\right) = \left[\begin{array}{ccc} \mathbf{A}^1\left(\mathbf{x}\right) & \mathbf{A}^2\left(\mathbf{x}\right) & \mathbf{A}^3\left(\mathbf{x}\right) \end{array} \right] , \tag{7}$$

with

$$\mathbf{A}^1\left(\mathbf{x}\right) = \left[\begin{array}{ccc} x_1 & 0 & \frac{1}{2}x_2 \\ 0 & x_2 & \frac{1}{2}x_1 \end{array} \right] , \tag{8}$$

$$\mathbf{A}^2\left(\mathbf{x}\right) = \left[\begin{array}{cc} -\alpha_1 x_1 x_2 & -\alpha_2 \frac{1}{2}\left(x_2^2 + \nu_{12}x_1^2\right) \\ \frac{1}{2}\alpha_1\left(x_1^2 + \lambda_1\nu_{12}x_2^2\right) & \alpha_2 x_1 x_2 \end{array} \right] , \tag{9}$$

$$\mathbf{A}^3\left(\mathbf{x}\right) = \alpha_3 s \left[\begin{array}{c} 3b_1 x_1^2 x_2 + c_1 x_2^3 \\ -3b_2 x_1 x_2^2 - c_2 x_1^3 \end{array} \right] , \tag{10}$$

In formulas (8)-(10), it is set $\lambda_1 = e_2/e_1$, e_1 and e_2 are the Young's moduli of the equivalent homogenized orthotropic material, ν_{12} the Poisson ratio and:

$$\begin{array}{ll} b_1 = \lambda_1 + \rho^2\nu_{12}, & c_1 = \rho^2 + \nu_{12} - \lambda_2, \\ b_2 = \rho^2 + \nu_{12}, & c_2 = \rho^2\nu_{12} + \lambda_1 - \rho^2\lambda_2, \end{array} \tag{11}$$

where $\lambda_2 = e_2/g_{12}$, with g_{12} being the homogenized shear modulus, while $\rho = a_2/a_1$ is the ratio between the dimensions of the UC and

$$s = \frac{10\left(1+\rho^2\right)}{a_1^2\left\{\lambda_1 + \rho^2\left[\left(\nu_{12} - \lambda_2\right)\left(1+\rho^2\right) + \rho^4\right]\right\}} . \tag{12}$$

The quantities α_1, α_2 and α_3 allow to take into account the influence of the perturbation parts of the displacement field in the determination of the average macroscopic strains. In particular, it results that:

$$\alpha_1 = 1 - \frac{k_1}{K_1} , \qquad \alpha_2 = 1 - \frac{k_2}{K_2} , \qquad \alpha_3 = 1 - \frac{f}{\Theta} , \tag{13}$$

where k_1, k_2 and f are terms explicitly reported in [2].

3 Characterization of the perturbation field

The vector $\widetilde{\mathbf{u}}(\mathbf{X},\mathbf{x})$ introduced in Eq. (4) is an unknown perturbation field that accounts for the effects of heterogeneity and vanishes in the trivial case of a homogeneous material. In the case of the first order homogenization, $\widetilde{\mathbf{u}}(\mathbf{X},\mathbf{x})$ is a periodic fluctuation, thus periodic boundary conditions are suitable for solving the BVP on the UC. When, instead, higher order polynomials are included in the kinematic map, there is no reason for assuming periodic displacement and strain fluctuation fields and anti–periodic traction vectors at the boundary, as noticed in [8, 7, 2].

In this section, two different approaches to characterize the fluctuation field are introduced. The first technique, presented in Section 3.1, assumes the decomposition of the perturbation field $\widetilde{\mathbf{u}}(\mathbf{X},\mathbf{x})$ in different contributions, related to the first, second and third order gradients of the kinematic map. The second one, discussed in Section 3.2, is based on the imposition of proper boundary conditions (BCs) on the UC as described in [2]. A comparison between the numerical results obtained using the adopted procedures for a paradigmatic example of a two-phase composite material, characterized by cubic symmetry, is proposed in Section 3.3.

3.1 Micromechanical description of the heterogeneous medium: three steps homogenization

The procedure based on the methodology proposed in [8] is extended to the case of a 2D Cosserat medium at the macroscopic scale. In the following, the main steps of the proposed procedure are addressed, exploiting the superposition principle. Initially, only the first order terms of the kinematic map multiplying the vector $\overline{\mathbf{E}}$ in (6), are activated; subsequently, the effects of the quadratic terms related to $\mathbf{K}$ are considered and, finally, the third order term associated to Θ is taken into account.

When only the linear terms of the kinematic map are considered, the case of the first order homogenization is recovered. In this instance, considering $\mathbf{K}=\mathbf{0}$ and $\Theta=0$, the two terms defining the displacement field $\mathbf{u}(\mathbf{X},\mathbf{x})$ in (4) can be expressed as:

$$\mathbf{u}^{*}(\mathbf{X},\mathbf{x})=\mathbf{A}^{1}(\mathbf{x})\,\overline{\mathbf{E}}(\mathbf{X})\;,\qquad\qquad \widetilde{\mathbf{u}}(\mathbf{X},\mathbf{x})=\widetilde{\mathbf{r}}^{1}(\mathbf{X},\mathbf{x})\;, \tag{14}$$

where the perturbation term $\widetilde{\mathbf{r}}^{1}(\mathbf{X},\mathbf{x})$ is an unknown field.

Herein, it is assumed that $\widetilde{\mathbf{r}}^{1}(\mathbf{X},\mathbf{x})$ is evaluated as the product of unknown functions times the components of the first gradient of the kinematic map. In particular, the first gradient of the kinematic map is written in vectorial form as $\boldsymbol{\gamma}^{1}=\{u^{*}_{1,1},\,u^{*}_{1,2},\,u^{*}_{2,1},\,u^{*}_{2,1}\}^{T}$. Since it results $u^{*}_{1,2}=u^{*}_{2,1}$, only three components of $\boldsymbol{\gamma}^{1}$ are independent and the following reduced vector can be considered:

$$\overline{\boldsymbol{\gamma}}^{1}(\mathbf{X},\mathbf{x})=\{\varepsilon^{*}_{1}\quad\varepsilon^{*}_{2}\quad\gamma^{*}_{12}\}^{T} \tag{15}$$

Thus, it is assumed that the perturbation term is given by:

$$\widetilde{\mathbf{r}}^{1}(\mathbf{X},\mathbf{x})=\boldsymbol{\Lambda}^{1}(\mathbf{x})\,\overline{\boldsymbol{\gamma}}^{1}(\mathbf{X},\mathbf{x})\qquad\text{with}\quad\boldsymbol{\Lambda}^{1}(\mathbf{x})\;=\;\left[\;\boldsymbol{\Lambda}^{1}_{1}(\mathbf{x})\quad\boldsymbol{\Lambda}^{1}_{2}(\mathbf{x})\quad\boldsymbol{\Lambda}^{1}_{3}(\mathbf{x})\;\right] \tag{16}$$

$\mathbf{\Lambda}_i^1(\mathbf{x})$, $i = 1, 2, 3$, being evaluated by applying the components E_1, E_2 and Γ_{12} of the vector $\overline{\mathbf{E}}$, respectively.

When also the presence of the curvature vector $\mathbf{K}$ is considered, with $\Theta = 0$, the two terms defining the displacement field $\mathbf{u}(\mathbf{X}, \mathbf{x})$ in (4) can be expressed as:

$$\begin{aligned} \mathbf{u}^*(\mathbf{X}, \mathbf{x}) &= \mathbf{A}^1(\mathbf{x})\,\overline{\mathbf{E}}(\mathbf{X}) + \mathbf{A}^2(\mathbf{x})\,\mathbf{K}(\mathbf{X}) \,, \\ \widetilde{\mathbf{u}}(\mathbf{X}, \mathbf{x}) &= \mathbf{\Lambda}^1(\mathbf{x})\,\overline{\boldsymbol{\gamma}}^1(\mathbf{X}, \mathbf{x}) + \widetilde{\mathbf{r}}^2(\mathbf{X}, \mathbf{x}) \,, \end{aligned} \tag{17}$$

where $\widetilde{\mathbf{r}}^2(\mathbf{X}, \mathbf{x})$ is the only unknown field. Following the same procedure as for the first term $\widetilde{\mathbf{r}}^1(\mathbf{X}, \mathbf{x})$, it is assumed that the function $\widetilde{\mathbf{r}}^2(\mathbf{X}, \mathbf{x})$ is expressed as the product of unknown functions and the components of the first gradient of $\overline{\boldsymbol{\gamma}}^1(\mathbf{X}, \mathbf{x})$, which is arranged in the vector $\boldsymbol{\gamma}^2 = \{\varepsilon^*_{1,1},\, \varepsilon^*_{1,2},\, \varepsilon^*_{2,1},\, \varepsilon^*_{2,1},\, \gamma^*_{12,1},\, \gamma^*_{12,2}\}^T$. Since it results $\gamma^*_{12,1} = \gamma^*_{12,2} = 0$, the only nonvanishing components of $\boldsymbol{\gamma}^2$ are arranged in the following vector:

$$\overline{\boldsymbol{\gamma}}^2(\mathbf{X}, \mathbf{x}) = \left\{\varepsilon^*_{1,1} \quad \varepsilon^*_{1,2} \quad \varepsilon^*_{2,1} \quad \varepsilon^*_{2,2}\right\}^T . \tag{18}$$

Then, the unknown field $\widetilde{\mathbf{r}}^2(\mathbf{X}, \mathbf{x})$ is represented in the form:

$$\widetilde{\mathbf{r}}^2(\mathbf{X}, \mathbf{x}) = \mathbf{\Lambda}^2(\mathbf{x})\,\overline{\boldsymbol{\gamma}}^2(\mathbf{X}, \mathbf{x}) \quad \text{with } \mathbf{\Lambda}^2(\mathbf{x}) = \left[\begin{array}{cccc} \mathbf{\Lambda}_1^2(\mathbf{x}) & \mathbf{\Lambda}_2^2(\mathbf{x}) & \mathbf{\Lambda}_3^2(\mathbf{x}) & \mathbf{\Lambda}_4^2(\mathbf{x}) \end{array}\right] \tag{19}$$

$\mathbf{\Lambda}_i^2(\mathbf{x})$, $i = 1, .., 4$, being functions evaluated by applying the components K_1 and K_2.

Finally, when the component Θ is taken into account, it results:

$$\begin{aligned} \mathbf{u}^*(\mathbf{X}, \mathbf{x}) &= \mathbf{A}^1(\mathbf{x})\,\overline{\mathbf{E}}(\mathbf{X}) + \mathbf{A}^2(\mathbf{x})\,\mathbf{K}(\mathbf{X}) + \mathbf{A}^3(\mathbf{x})\,\Theta(\mathbf{X}) \,, \\ \widetilde{\mathbf{u}}(\mathbf{X}, \mathbf{x}) &= \mathbf{\Lambda}^1(\mathbf{x})\,\overline{\boldsymbol{\gamma}}^1(\mathbf{X}, \mathbf{x}) + \mathbf{\Lambda}^2(\mathbf{x})\,\overline{\boldsymbol{\gamma}}^2(\mathbf{X}, \mathbf{x}) + \widetilde{\mathbf{r}}^3(\mathbf{X}, \mathbf{x}) \,. \end{aligned} \tag{20}$$

The unknown function $\widetilde{\mathbf{r}}^3(\mathbf{X}, \mathbf{x})$ is written as product of unknown functions and the components of the first gradient of $\overline{\boldsymbol{\gamma}}^2(\mathbf{X}, \mathbf{x})$, which is arranged in the vector:

$$\boldsymbol{\gamma}^3 = \{\varepsilon^*_{1,11},\, \varepsilon^*_{1,12},\, \varepsilon^*_{1,21},\, \varepsilon^*_{1,22},\, \varepsilon^*_{2,11},\, \varepsilon^*_{2,12},\, \varepsilon^*_{2,21},\, \varepsilon^*_{2,22}\}^T .$$

As in the previous cases, only the relevant and nonvanishing components of $\boldsymbol{\gamma}^3$ are collected into the reduced vector:

$$\overline{\boldsymbol{\gamma}}^3(\mathbf{X}, \mathbf{x}) = \left\{\begin{array}{c} \varepsilon^*_{1,12} \\ \varepsilon^*_{2,12} \\ \gamma^*_{12,12} \end{array}\right\} . \tag{21}$$

Again, the unknown vector $\widetilde{\mathbf{r}}^3(\mathbf{X}, \mathbf{x})$ is written as:

$$\widetilde{\mathbf{r}}^3(\mathbf{X}, \mathbf{x}) = \mathbf{\Lambda}^3(\mathbf{x})\,\overline{\boldsymbol{\gamma}}^3(\mathbf{X}, \mathbf{x}) \quad \text{with } \mathbf{\Lambda}^3(\mathbf{x}) = \left[\begin{array}{ccc} \mathbf{\Lambda}_1^3(\mathbf{x}) & \mathbf{\Lambda}_2^3(\mathbf{x}) & \mathbf{\Lambda}_3^3(\mathbf{x}) \end{array}\right] \tag{22}$$

$\mathbf{\Lambda}_{\mathrm{i}}^3(\mathbf{x})$, $i = 1, .., 3$, being functions evaluated by applying the components Θ.

Finally, the total fluctuation displacement vector $\widetilde{\mathbf{u}}(\mathbf{X},\mathbf{x})$ can be expressed as the sum of three fields evaluated in sequence (three-steps homogenization), according to formulas (16), (19) and (22):

$$\begin{aligned}\widetilde{\mathbf{u}}(\mathbf{X},\mathbf{x}) &= \widetilde{\mathbf{r}}^1(\mathbf{X},\mathbf{x}) + \widetilde{\mathbf{r}}^2(\mathbf{X},\mathbf{x}) + \widetilde{\mathbf{r}}^3(\mathbf{X},\mathbf{x}) &(23)\\ &= \boldsymbol{\Lambda}^1(\mathbf{x})\,\overline{\boldsymbol{\gamma}}^1(\mathbf{X},\mathbf{x}) + \boldsymbol{\Lambda}^2(\mathbf{x})\,\overline{\boldsymbol{\gamma}}^2(\mathbf{X},\mathbf{x}) + \boldsymbol{\Lambda}^3(\mathbf{x})\,\overline{\boldsymbol{\gamma}}^3(\mathbf{X},\mathbf{x})\ . &(24)\end{aligned}$$

Similarly to [8, 5], it is assumed that the functions $\boldsymbol{\Lambda}^j(\mathbf{x})$ $(i = 1, 2, 3)$ satisfy the periodicity conditions in the UC.

3.2 Distribution of the perturbation field: boundary conditions on the UC

The characterization of the perturbation field $\widetilde{\mathbf{u}}$ is performed in [2] by observing its actual distribution. To this end, a RVE obtained as assemblage of a large number of UCs for a selected two-phase periodic composite material is considered and remote fully displacement BCs are prescribed. In particular, the Cosserat deformation modes are imposed on the boundary and the RVE response is evaluated by finite element method. Hence, the distribution of the perturbation field arising in the central UC of the RVE is taken as benchmark. In fact, it is assumed as the actual field occurring in the composite, when second and third order polynomial displacement fields related to the additional Cosserat strain components are assigned, according to the terms of the kinematic map in Eq. (6). Thus, the problem of the derivation of the suitable BCs to impose on a single UC, in order to reproduce with a satisfactory level of accuracy the actual distribution of the perturbation field, is investigated.

In particular, some selected two-phase composite materials, characterized by material symmetries ranging from cubic to orthotropic are analyzed.

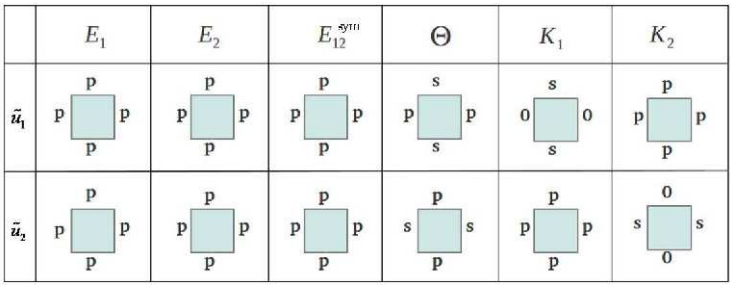

Figure 1: Boundary conditions required for 2D Cosserat strain components.

In all the considered cases, similar distributions of the perturbation displacement fields on the UC boundary emerge. Differently from the case of the first order homogenization procedure, where periodic BCs are suitably adopted, in the analyzed cases more complex BCs have to be considered, which are different for the two components of $\widetilde{\mathbf{u}}$. In Figure 1 the derived BCs are summarized. In the first row, the applied Cosserat macroscopic

deformation components are reported; in the second row the boundary conditions for the component $\widetilde{u}_1$ along the horizontal and vertical edges of the UC are schematically reported, while in third row those for the displacement component $\widetilde{u}_2$ are shown. The symbol "p" indicates periodic BCs; "s" skew-periodic BCs, while "0" indicates zero perturbation displacement BCs.

3.3 Perturbation displacement fields: comparison between the proposed approaches

The approaches presented above to evaluate the perturbation field $\widetilde{\mathbf{u}}$ on the UC are compared by carrying out some numerical tests. Computations are performed by using classical Lagrangian bi-quadratic 8-node finite elements within the FEAP code [9].

Numerical analyses are developed for a two-phase composite material, characterized by cubic symmetry. The texture is made of a soft matrix with stiff square inclusions, both isotropic, regularly spaced and arranged as shown in Figure 2-1, where a RVE, obtained by periodic repetition of a large number of UCs, is represented. The ratio between the Young's moduli of the inclusions, e_i, and of the matrix, e_m, is set $e_i/e_m = 10^2$, while the same Poisson ratio $\nu = 0.3$ is used for both the materials. The volume fraction of inclusions is set equal to 36%.

In Figure 2-1, the dashed lines bound the central UC represented in Figure 2-2. Of course, the choice of the UC is not unique and different UCs can be selected, for example see 2-3. Micromechanical analyses concerning the components E_1, E_2 and Γ_{12} of the

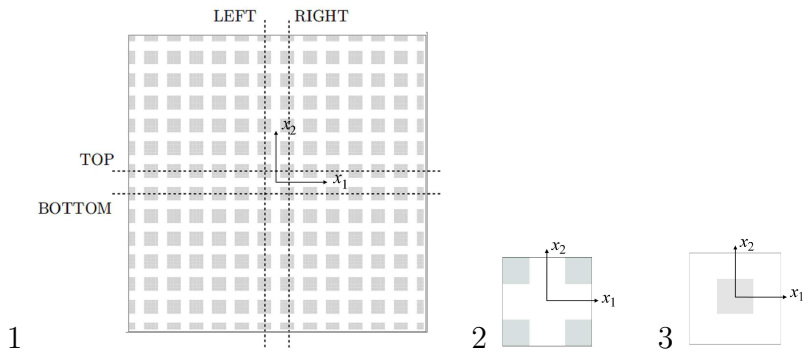

Figure 2: RVE of the two-phase composite material and UC considered for the composite material.

macroscopic Cosserat strain are standard and are not performed in the following. Thus, numerical analyses are carried out only for the components K_1, K_2 and Θ of $\mathbf{E}$. Thus, only the higher order polynomial terms of the kinematic map related to K_1, K_2 and Θ are considered.

Fully displacement BCs are imposed at the boundary of the RVE and the corresponding perturbation fields along the edges of the central UC are evaluated. These are compared with those obtained analyzing a single UC, in Figure 2-2, and applying the procedures

described in Sections 3.1 and 3.2, denoted in the following by $M1$ and $M2$, respectively.

The homogenized coefficients e_1, e_2 and g_{12}, required to define the kinematic map, are obtained by applying the first order homogenization procedure to the UC.

In all the reported figures solid lines correspond to the perturbation displacement fields evaluated at the boundary of the UC located at the center of the RVE, when remote fully displacement BCs are imposed. Dashed lines refer to those evaluated for the single UC, adopting the procedure $M1$ and dotted lines correspond to the results obtained imposing the boundary conditions deduced from the procedure $M2$. Moreover, the values of the displacements are normalized with respect to the maximum value in the UC of the correspondent component obtained from the kinematic map.

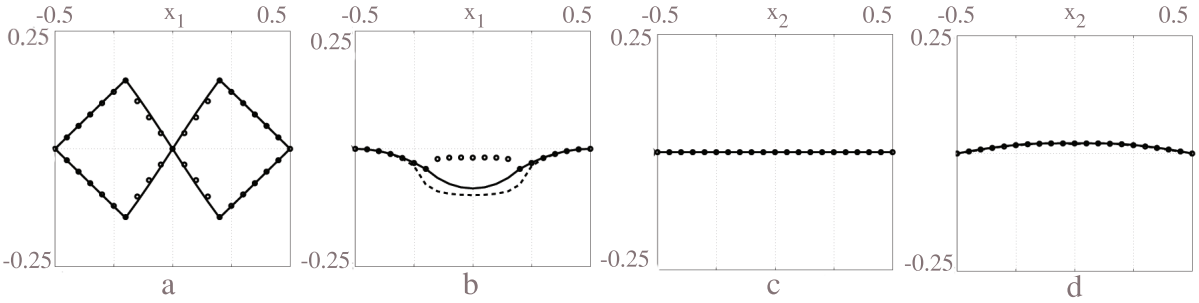

Figure 3: K_1 component on the UC in Figure 2: a) horizontal, b) vertical perturbation components along the horizontal lines, c) horizontal and d) vertical perturbation components along the vertical lines .

First of all, the case in which only $K_1 \neq 0$, while all the other macroscopic strain components vanish, is considered. In Figure 3-a and 3-b the horizontal and vertical perturbation components are plotted along the TOP and BOTTOM horizontal lines of the UC. No differences arise between the results for the horizontal component, while it is evident that a better approximation of the vertical component is obtained with $M1$ compared to $M2$. Instead, in 3-c and 3-d the three procedures lead to the same results for both horizontal and vertical components along the vertical lines (LEFT and RIGHT).

Finally, the case $\Theta \neq 0$ is considered and the results for the UC are illustrated in Figure 4. In this case, the horizontal and vertical perturbation components along the TOP and BOTTOM lines coincide with the vertical and horizontal components along the LEFT and RIGHT lines, respectively. Also considering this macro-strain component, there is an evident improvement in reproducing the displacement field of the RVE for all the considered components adopting the procedure $M1$.

4 Identification of the constitutive terms

The identification procedure adopted in this work is based on the generalized Hill-Mandel macrohomogeneity condition. The virtual work evaluated at the macroscopic

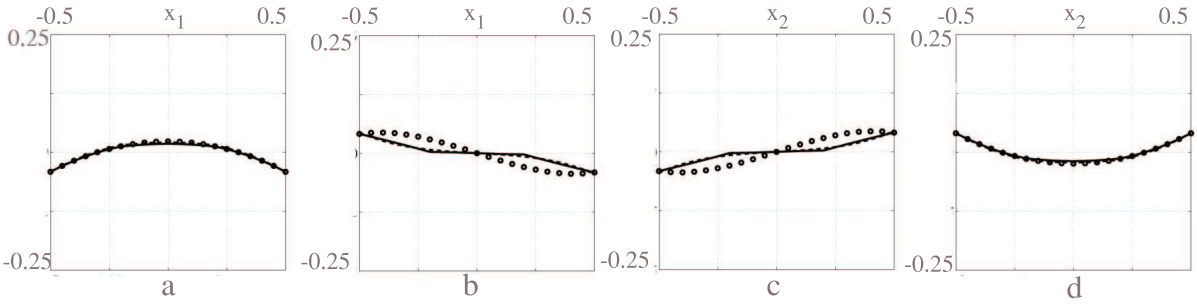

Figure 4: Θ component on the UC in Figure 2: a) horizontal, b) vertical perturbation components along the horizontal lines, c) horizontal and d) vertical perturbation components along the vertical lines .

Cosserat point is set equal to the average virtual work of the heterogeneous Cauchy material computed on the UC. Thus, the following expression holds:

$$\boldsymbol{\Sigma}^T \, \mathbf{E} = \left\langle \boldsymbol{\sigma}^T \, \boldsymbol{\varepsilon} \right\rangle_\omega \tag{25}$$

where $\boldsymbol{\Sigma}$ is the Cosserat stress vector evaluated at the macroscopic point, while $\boldsymbol{\sigma}$ is the Cauchy stress vector at the typical point of the UC. After solving the BVP on the UC and determining the microscopic strain and stress fields, $\boldsymbol{\varepsilon}$ and $\boldsymbol{\sigma}$, the homogenized Cosserat elastic constitutive matrix $\mathbf{C}$ can be identified by using Eq. (25). In particular, considering a two-phase periodic composite material with a regular arrangement of the inclusions, characterized by orthotropic texture, the homogenized Cosserat elastic constitutive matrix, expressed in a reference frame aligned with the principal axes of the material, results as:

$$\mathbf{C} = \begin{bmatrix} \mathbf{C}_1 & \mathbf{0} \\ \mathbf{0} & \mathbf{C}_2 \end{bmatrix} . \tag{26}$$

where $\mathbf{C}_1$ is a 3×3 matrix collecting the standard Cauchy coefficients C_{11}, C_{22}, C_{12} and C_{33}, related to the Cauchy part of the strain $\mathbf{E}$, $\mathbf{C}_2$ is a diagonal 3×3 matrix containing the constants C_{44}, C_{55} and C_{66} governing the bending and skew-symmetric shear behavior of the Cosserat equivalent medium, and $\mathbf{0}$ is a 3×3 zero matrix. Here, the attention is focused on the determination of C_{44}, C_{55} and C_{66}.

Aiming at determining the coefficient C_{44}, the macroscopic strain component K_1 is applied to the UC. For the two UCs in Figure 2-2 and 2-3, the constitutive coefficient C_{44} is evaluated and reported in Table 1-1, by using both the above presented procedures $M1$ and $M2$. Note that, due to the cubic symmetry of the composite material, the case $\alpha_2 K_2 = 1$ leads to results which are the rotated of the case $\alpha_1 K_1 = 1$, so that it is $C_{55} = C_{44}$. It results that the two adopted methods, $M1$ and $M2$, lead to homogenized constitutive parameters that differ by about 8% for the same UC. Moreover, contrarily to what is expected for periodic media, it emerges that the obtained results depend on

1

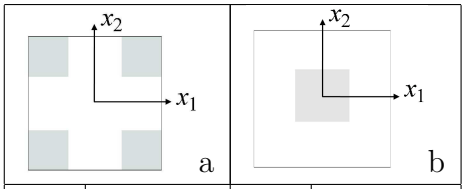

	C_{44}		C_{44}
$M1$	19.5	$M1$	16.8
$M2$	21.1	$M2$	15.36

2

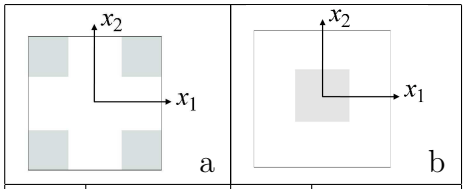

	C_{66}		C_{66}
$M1$	5366	$M1$	3003
$M2$	6210	$M2$	2310

Table 1: Constitutive coefficient C_{44} evaluated in the UC for $\alpha_1 K_1 = 1$ adopting $M1$ and $M2$ for the solution of the BVP.

the choice of the UC. Indeed, the values of C_{44} computed for the two UCs differ by 14%, when the method $M1$ is adopted, and about 27% when the method $M2$ is employed. The dependence of the identified coefficient C_{44} on the choice of the UC can be reasonably related to the adopted polynomial kinematic map as well as to the identification procedure. Further numerical tests are performed to investigate on the influence of the size of the RVE. In fact, various square RVEs are considered, taking into account assemblages of 3×3, 5×5, ..., 15×15 UCs, subjected to the boundary conditions shown in Figure 1, which correspond to the $M2$ methodology illustrated in Section 3.2. The averaged internal work is evaluated over the entire RVE domains.

To be noted is that, as the RVE size increases, the values of C_{44} (scaled by factor L^2 with L the size of the square RVE) converge to the same quantity, from above and from below, respectively. Moreover, a quite fast convergence rate of C_{44} emerges. Similar considerations apply in relation to the application of the component Θ such that $\alpha_3\Theta = 1$, while all the other macro-level strain components are set equal to zero.For the two UCs in Figure 2-2 and 2-3, the constitutive coefficient C_{66} is evaluated and reported in Table 1-2, by using both the above presented procedures $M1$ and $M2$.

5 CONCLUSIONS

The characterization the perturbation fields in presence of higher order polynomial boundary conditions is performed via a micromechanical three-steps computational homogenization. The results obtained by analyzing a single UC, proper selected for the composite analyzed, are in a very good agreement with the reference solution evaluated on the RVE of the material. The observed little discrepancies are due to the lacking in fully satisfying the kinematic compatibility between the adjacent UCs. Furthermore, the perturbation fields, evaluated by applying on the UC the BCs derived in [2] and reported for comparison, match worst the reference solution, although the results are satisfactory taking into consideration the simplicity of the procedure.

Moreover, in the paper the identification of the homogenized linear elastic constitutive parameters is investigated. Reference was made to the additional Cosserat components, thus relating Θ, K_1 and K_2 to the work-conjugated stresses, for the studied two-phase

composite material. The classical Hill-Mandel procedure was adopted. By analyzing to different UCs, selected for representing the composite texture, it emerged that the constitutive response of the homogenized UC depends on the choice of the cell itself, at odds with what expected. To obtain an objective response, it is necessary to resort to a RVE made of an assemblage of UCs, which is equivalent to the average of the responses of the different single UCs. On the other hand, the obtained results were put into question by the observation the values identified for the constitutive parameters of the homogenized Cosserat continuum, at least in the case analyzed, coincide with those evaluated by simply considering at the micro-level a homogenized Cauchy medium. It is reasonable to relate these undesired results both to the adopted kinematic map and to the Hill-Mandel identification technique. Hence, it appears relevant to carry on further developments, focusing on the formulation of the link between the macro- and micro-levels, as well as on the improvement of the identification procedure.

REFERENCES

[1] M. De Bellis, D. Addessi, A Cosserat based multi-scale model for masonry structures, Int J Multiscale Com 9 (5) (2011) 543–563.

[2] D. Addessi, M. L. De Bellis, E. Sacco, Micromechanical analysis of heterogeneous materials subjected to overall cosserat strains, Mech Res Commun 54 (2013) 27–34.

[3] S. Forest, K. Sab, Cosserat overall modeling of heterogeneous materials, Mech Res Commun 25 (1998) 449–454.

[4] V. G. Kouznetsova, M. G. D. Geers, W. A. M. Brekelmans, Multi-scale second-order computational homogenization of multi-phase materials: a nested finite element solution strategy, Computer Methods in Applied Mechanics and Engineering 193 (48-51) (2004) 5525–5550.

[5] A. Bacigalupo, L. Gambarotta, Second-order computational homogenization of heterogeneous materials with periodic microstructure, ZAMM-Z Angew Math Me 90 (11) (2011) 796–811.

[6] D. Addessi, E. Sacco, A multi-scale enriched model for the analysis of masonry panel, Int J Solids Struct 49 (2012) 865–880.

[7] S. Forest, D. Trinh, Generalized continua and non-homogeneous boundary conditions in homogenisation methods, ZAMM-Z Angew Math Me 91 (2) (2011) 90–109.

[8] X. Yuan, Y. Tomita, T. Andou, A micromechanical approach of nonlocal modeling for media with periodic microstructures, Mech Res Commun 35 (1–2) (2008) 126 – 133.

[9] R. Taylor, FEAP-A finite element analysis program, Version 8.3, Department of Civil and Environmental Engineering, University of California at Berkeley, California, 2011.